Earth Planet. Sci. Lett. 671 (2025) 119650



Contents lists available at ScienceDirect

Earth and Planetary Science Letters

journal homepage: www.elsevier.com/locate/epsl



A lower mantle origin for the young mare basalts returned by Chang'e-5?

Runwu Li [a,b,*], Ming Tang [a,b], Jiaxi Wang [a]

[a] Key Laboratory of Orogenic Belt and Crustal Evolution, MOE, School of Earth and Space Sciences, Peking University, Beijing 100871, China
[b] Research Institute of Extraterrestrial Material (RIEMPKU), School of Earth and Space Sciences, Peking University, Beijing 100871, China

ARTICLE INFO

Edited by Dr Fang-Zhen Teng

Keywords:
Chang'e-5 basalts
Garnet
High pressure
Lunar lower mantle

ABSTRACT

The samples returned by the recent Chang'e-5 (CE-5) mission confirmed active lunar magmatism at least two billion years ago, which challenged the long-held view of an inactive Moon through much of its lifespan. However, the origin of this extended lunar magmatism remains mysterious. The CE-5 lunar soil and basalt fragments exhibit a strong fractionation between middle and heavy rare earth elements, a phenomenon rarely observed in the Apollo samples. We confirm this fractionation as a primary magmatic signature with measurements of the pyroxenes. By coupling phase equilibria modeling and element partitioning calculations, we show that this fractionation can only be produced if the magma source contained ~5-10% garnet at a minimum depth of ~700 km. We suggest the primary CE-5 magma may have originated from the lunar lower mantle. For melting to occur, one possibility is that convection may have been sustained in the deep lunar mantle until at least two billion years ago. Alternatively, the CE-5 magma may have tapped the melt-bearing layer near the core, as indicated by recent seismic observations.

1. Introduction

Lunar mare basalts are derived from the partial melting of mantle cumulates formed at various depths during the crystallization of the lunar magma ocean (LMO) and subsequent mantle overturn processes (Borg and Carlson, 2023; Neal and Taylor, 1992; Snyder et al., 1992). These basalts serve as a direct record of the Moon's magmatic evolution, and their petrogenesis plays a crucial role in reconstructing the thermo-chemical evolution of the lunar interior (Shearer et al., 2006; Wieczorek et al., 2006). Radiometric dating of mare basalts collected from the Apollo and Lunar mission landing sites suggests ages ranging from approximately 4.3 to 3.1 Ga (Snape et al., 2019). The recent Chang'e-5 (CE-5) mission, which landed in the northern Oceanus Procellarum within the Procellarum KREEP Terrane (PKT), returned the youngest (~2.0 Ga) lunar basalts confirmed to date (Che et al., 2021; Li et al., 2021b). While the early volcanic activity (~4.3–3.1 Ga) is relatively straightforward to explain from a thermal perspective, the later stages of volcanism (~2.0 Ga) present a more complex challenge, as the Moon, a relatively small body, would be expected to cool rapidly (Spohn et al., 2001). Geochemical analyses of CE-5 basalts indicate that they originate from low-degree partial melting of a dry, limited-KREEP (< 0.5 %) mantle source, followed by extensive fractional crystallization (Hu et al., 2021; Tian et al., 2021). These characteristics exclude two potential mechanisms—radiogenic heating and hydrous melting—as primary drivers of the young volcanism.

To explain the generation of these young mare basalts on a cooling Moon, various source models have been proposed. These include orthopyroxene-rich cumulates with contributions from ilmenite-bearing cumulates (IBC) (Su et al., 2022, 2023), and clinopyroxene-rich cumulates, either with or without contributions from IBC (Haupt et al., 2023; Luo et al., 2023; Wang et al., 2024a). The presence of easily melted IBC components in the CE-5 mantle source has been suggested to lower the mantle's melting point, potentially playing a key role in driving late-stage lunar volcanism (Su et al., 2023). Earlier studies have also estimated the melting conditions of the CE-5 basalt mantle source. While these estimates vary, they generally place the melting depth in the upper mantle, ranging from ~4 kbar (<100 km) to ~2.5 GPa (~550 km) (Luo et al., 2023; Su et al., 2022; Wang et al., 2024a). These depth estimates were derived either by determining the multiple saturation points (MSP) of the assumed primary magmas or using mineral thermobarometers. However, given that the CE-5 basalts are products of extensive crystal fractionation (Tian et al., 2021), mineral thermobarometers may not be suitable for estimating the melting pressure at the mantle source. In addition, the choice of assumed primary magma composition can significantly influence the estimation of melting pressure. These factors likely account for the considerable variability in the estimated melting

* Corresponding author.
E-mail address: runwu.lee@pku.edu.cn (R. Li).

https://doi.org/10.1016/j.epsl.2025.119650
Received 8 April 2025; Received in revised form 10 September 2025; Accepted 20 September 2025
0012-821X/© 2025 Elsevier B.V. All rights are reserved, including those for text and data mining, AI training, and similar technologies.

pressures discussed above.

One intriguing observation, though largely overlooked in previous studies, is that the CE-5 samples exhibit strongly fractionated rare earth elements (REEs) (Fig. 1A). According to previous analyses (Li et al., 2021a; Wang et al., 2024b), the CE-5 soils and bulk basalt fragments both show substantial fractionation between middle and heavy REEs, as evidenced by their high $(Sm/Yb)_N$ ratios (where N indicates chondrite-normalized) of 1.9–2.1 (Fig. 1B). In contrast, the mare basalts returned by the Apollo missions—including low-Ti, and high-Ti groups—generally display lower $(Sm/Yb)_N$ ratios than the CE-5 samples, with the low-Ti groups showing higher $(Sm/Yb)_N$ ratios than the high-Ti group (Fig. 1). The KREEP basalts show higher $(Sm/Yb)_N$ values than the Apollo mare basalts, but still lower than the CE-5 basalts on average (Fig. 1). In addition to the high $(Sm/Yb)_N$ ratios, the CE-5 samples show notable enrichments in light REEs, reflected in their elevated $(La/Sm)_N$ ratios (Figs. 1A and 1C). Strong fractionation between REEs, particularly between middle and heavy REEs, is often regarded as a sign of garnet fractionation (Chen et al., 2023; Tang et al., 2020). Garnet fractionation is also consistent with the low Lu/Hf ratios (~0.1) in CE-5 samples compared to those of the Apollo basalts (averaging 0.16 ± 0.03, 2 SD) (Warren and Taylor, 2014).

In this study, we focus on the strongly fractionated REEs in the CE-5 samples. We first conducted in-situ trace element measurements of pyroxenes from the CE-5 basalts and compiled existing geochemical data for the CE-5 and Apollo samples. Then, by integrating phase equilibria modeling with element partitioning calculations, we evaluated the roles of garnet fractionation and other processes in the generation of the CE-5 basalts and constrained the CE-5 mantle source depth. Finally, we explored the implications for dynamics of lunar deep mantle based on our findings.

2. Samples and methods

Given the potential heterogeneity issue introduced by the small sizes of basalt fragments, we carried out in-situ measurements of clinopyroxene, the major REE-bearing phase. Three basalt fragments (CE5C000YJYX147GP, CE5ZQ403YXYJ004GP, and CE5C0000YJYX050) from the CE-5 soil samples were selected in this study. They are mainly composed of pyroxene, olivine, plagioclase, and ilmenite (Fig. S1). We employed the Tescan Integrated Mineral Analyzer (TIMA) (EDAX Element 30) at the Key Laboratory of Orogenic Belts and Crustal Evolution, School of Earth and Space Sciences, Peking University, to examine the mounted rock fragments and identify clinopyroxene grains. The TIMA system consists of a Tescan Mira Schottky field emission scanning electron microscope equipped with four silicon drift energy dispersive spectrometer (EDS) detectors, arranged at 90° intervals around the sample chamber. The analysis was carried out at 25 kV, with a spot size of 98.77 nm, a working distance of 15 mm, and a field size of 400 μm, using the high-resolution liberation analysis mode. BSE images were collected to delineate the phase boundaries (Fig. S1).

Major and trace elements of clinopyroxene were analyzed using laser ablation-inductively coupled plasma-mass spectrometry (LA-ICP-MS) at the Key Laboratory of Orogenic Belts and Crustal Evolution, School of Earth and Space Sciences, Peking University. All measurements were conducted in spot mode, with a laser beam diameter of 24 μm, an ablation frequency of 5 Hz, and an energy density of approximately 4 J

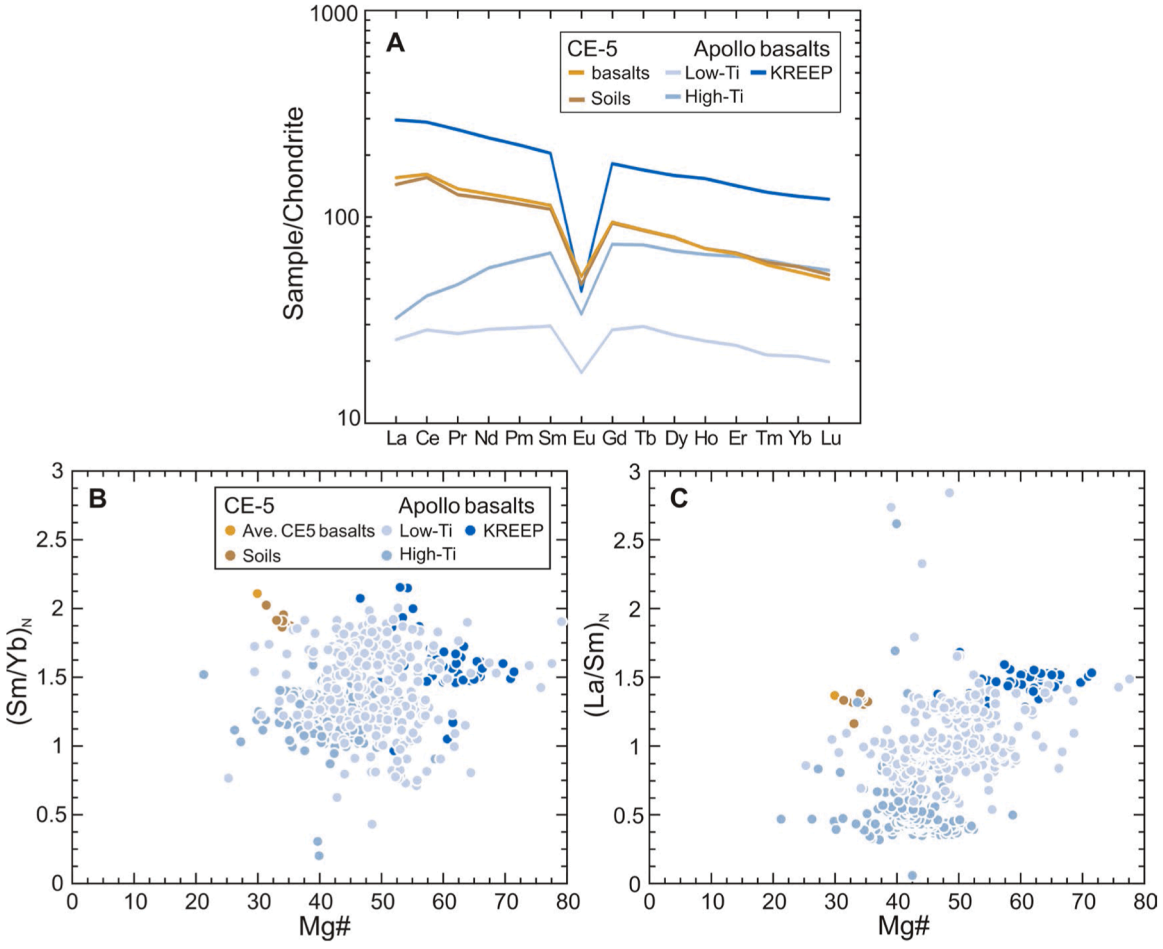


Fig. 1. Whole-rock average REE patterns (A) and whole-rock $(Sm/Yb)_N$ (B) and $(La/Sm)_N$ (C) versus Mg# diagrams for CE-5 samples and Apollo basalts. The chondrite REE data is from Sun and McDonough (1989). Compiled whole-rock geochemical data are provided in Table S1.

cm-2. Each analysis consisted of a 45-second background count followed by a 50-second count with the laser activated. The andesitic glass OJY-1 was employed as the calibration reference material (Wu et al., 2022). Two reference materials, GOR132 (Jochum et al., 2006) and ARM-1 (Wu et al., 2019), were measured to evaluate the accuracy of our analyses. The sum of all major element oxides was assumed to be 100 % and used as the internal standard. Data reduction was performed using the method outlined by Liu et al. (2008). The data are provided in Table S2.

3. Results

Pyroxenes (augite) in three basalt fragments from the CE-5 samples were analyzed for major and trace element contents simultaneously using LA-ICP-MS ($n = 60$). Our results, in conjunction with previously compiled data, show that the pyroxenes from the CE-5 basalts exhibit a broad compositional range, with Mg# values (atomic Mg/(Mg+Fe)) spanning from approximately 60 to 10, generally lower than those observed in the Apollo low-Ti basalts (Mg# ~70 to 10; Fig. 2). This suggests that the CE-5 basalts likely underwent some degree of crystal differentiation. Notably, the pyroxenes in the CE-5 basalts exhibit significantly more fractionated REE patterns compared to those in the Apollo samples, as evidenced by consistently higher $(Sm/Yb)_N$ and $(La/Sm)_N$ ratios across the full Mg# range (Fig. 2). The high $(Sm/Yb)_N$ ratios in the CE-5 pyroxenes imply that the equilibrium melts were strongly enriched in middle REEs relative to heavy REEs, considering that pyroxene exhibits partition coefficients for heavy REEs that are comparable to or higher than those for middle REEs (Fig. S43). We estimated melt compositions using compiled pyroxene–melt partition coefficients (Table S3). The calculated $(Sm/Yb)_N$ and $(La/Sm)_N$ ratios average 1.8 ± 0.8 and 1.2 ± 1.0 (2 SD), respectively (Fig. S2), systematically higher than those of Apollo pyroxenes and broadly consistent with values from CE-5 basalts and soils (Fig. S2). The somewhat large variability in $(Sm/Yb)_N$ and $(La/Sm)_N$ of the pyroxenes may result from local melt heterogeneities and disequilibrium partitioning due to rapid crystallization (Lee et al., 2022; Watson and Müller, 2009). Given these uncertainties, we adopt the CE-5 whole-rock average as a more robust estimate for the melt composition, as was done by most researchers (Su et al., 2022; Wang et al., 2024b; Zong et al., 2022). Furthermore, pyroxene $(Sm/Yb)_N$ and $(La/Sm)_N$ ratios show no systematic trend with decreasing Mg# (Fig. 2), which suggests limited influence from crystal fractionation processes.

4. Discussion

Our in-situ measurements of pyroxenes in the CE-5 samples confirm the high $(Sm/Yb)_N$ and $(La/Sm)_N$ ratios as a character of the CE-5 magma. Such strong fractionations were rarely observed in the Apollo mare basalts. Below, we evaluate what processes may have generated the high $(Sm/Yb)_N$ and $(La/Sm)_N$ ratios in the CE-5 magma.

4.1. Effects of magma crystal fractionation

The CE-5 basalts underwent relatively high degrees of crystal fractionation (Su et al., 2022; Tian et al., 2021). Recent studies of CE-5 clinopyroxenes suggest that the crystal fractionation of the CE-5 magma predominantly occurred in the shallow regions at the top of the lunar mantle (~2–5 kbar) (Luo et al., 2023). To assess whether the highly fractionated REE patterns resulted from extensive crystallization, we coupled rhyolite-MELTS simulations (Gualda et al., 2012) with trace element modeling to examine their impact on the $(Sm/Yb)_N$ ratios. Both calculations were conducted in fractional crystallization mode (See Text S1). The composition of the primary CE-5 melts is difficult to constrain precisely, but as a proof of concept, we considered a variety of primary CE-5 melt major element compositions (Grove et al., 1973; Su et al., 2023) for our evaluation (Fig. S3).

Using mineral phase proportions derived from the rhyolite-MELTS simulations, we calculated the $(Sm/Yb)_N$ and $(La/Sm)_N$ differentiation paths. The results indicate that these ratios remain nearly constant, even with high-degree fractional crystallization (>50 %) (Fig. 3). Similarly, the $(Sm/Yb)_N$ and $(La/Sm)_N$ ratios of the CE-5 pyroxenes show no discernible trend as Mg# decreases (Fig. 2). We thus conclude that the highly fractionated REEs of CE-5 basalts may reflect the characteristics of their primary melts rather than the result of crystal fractionation.

Another complexity stems from the re-equilibration between the primary melts and the shallow mantle during the ascent. This process, however, would likely attenuate the fractionated REE signature because of the lower pressure of re-equilibration. As a result, the $(Sm/Yb)_N$ ratios in the CE-5 primary melts are likely even higher than that of the CE-5 magma erupted at the surface.

4.2. KREEP addition

The final remnants of LMO are enriched in incompatible trace elements, specifically in K, REEs, and P, which was termed as "KREEP" (Warren and Wasson, 1979). This component exhibits relatively fractionated REE patterns, and the incorporation of KREEP (1–1.5 %) into the CE-5 mantle sources has been proposed to explain the fractionated REE patterns observed in the CE-5 basalts (Wang et al., 2024b; Zong et al., 2022). However, even with the highest KREEP content (1.5 %), the resulting melt has a $(Sm/Yb)_N$ ratio of 1.45 (Zong et al., 2022), significantly lower than the observed value in CE-5 basalts (Fig. 1B). Moreover, adding a high content of KREEP component in the source appears inconsistent with the radiogenic Sm-Nd isotope compositions of the CE-5 basalts (Tian et al., 2021). In addition, the average $(Sm/Yb)_N$ ratio of the

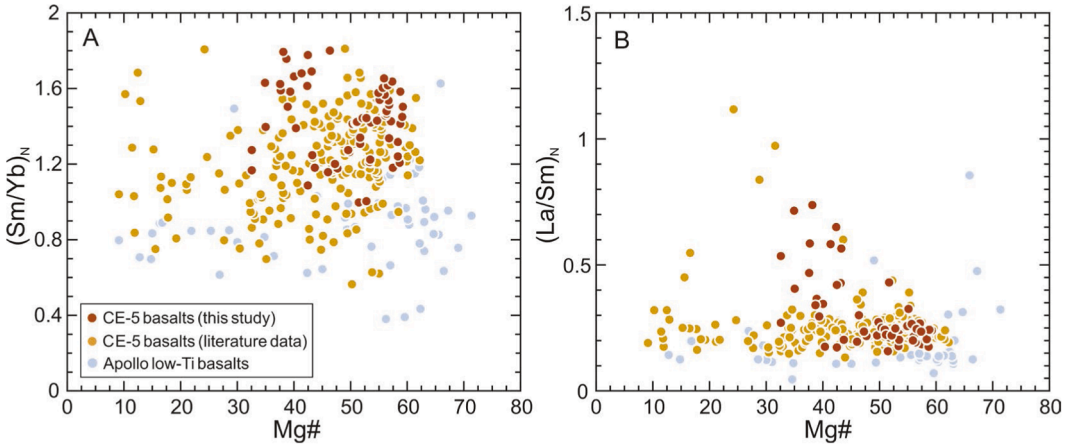


Fig. 2. Pyroxene (augite) $(Sm/Yb)_N$ (A) and $(La/Sm)_N$ (B) versus Mg# for CE-5 samples and Apollo basalts. Data for pyroxenes are provided in Tables S1 and S2.

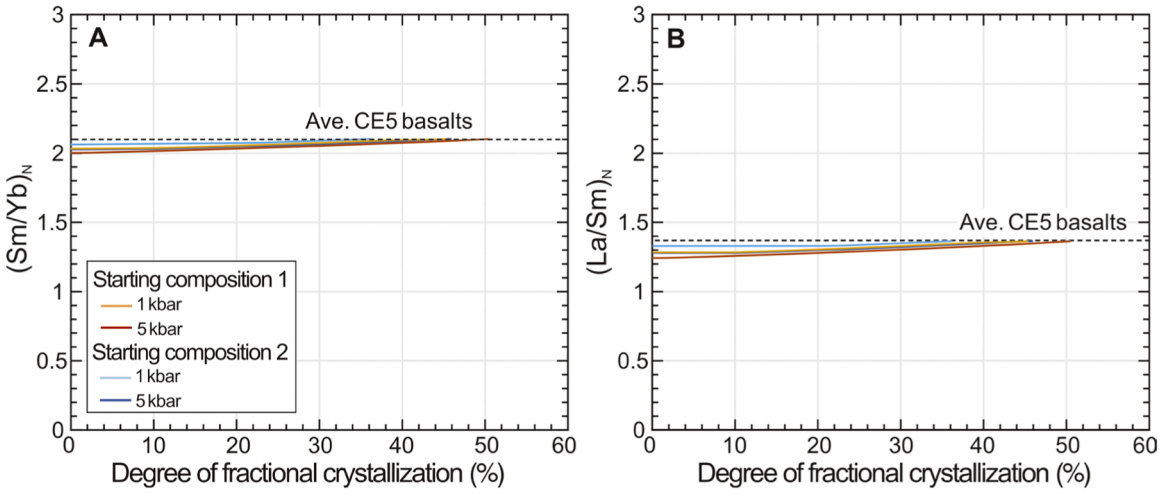


Fig. 3. Modeled $(Sm/Yb)_N$ (A) and $(La/Sm)_N$ (B) differentiation paths for two different CE-5 primary melt compositions. Starting compositions 1 and 2 are from Grove et al. (1973) and Su et al. (2023), respectively. Isobaric fractional crystallization was modeled for each composition. Based on previous pressure estimates of the main phase of CE-5 crystallization (~2–5 kbar; Luo et al., 2023), simulations were conducted at 1 and 5 kbar. The results of rhyolite-MELTS simulations and trace element calculations are listed in Table S4.

CE-5 basalts (2.1) is markedly higher than that of typical KREEP compositions (~1.5) (Warren, 1989), suggesting that KREEP assimilation was unlikely to have had a dominant influence on the strongly fractionated REE signatures of the CE-5 basalts.

4.3. Garnet signature inherited from LMO crystallization

Phase equilibria and experimental studies indicate that garnet-bearing cumulates could form in the lowermost mantle during the crystallization of the LMO (Jing et al., 2022; Johnson et al., 2021). In this case, if the remaining LMO was in equilibrium with the garnet-bearing cumulates, later cumulates crystalized from this remaining LMO may exhibit fractionated REE signatures. These signatures, in turn, may be inherited by mare basalts formed from the melting of these later cumulates. However, the mineralogy of the deep mantle is highly dependent on the bulk composition of the LMO and temperature and pressure conditions during its crystallization (Jing et al., 2022; Rapp and Draper, 2018). More uncertain is whether the early stage of LMO crystallization was predominantly in equilibrium or fractional, or when LMO crystallization transitioned from equilibrium to fractional (Elardo et al., 2011; Schmidt and Kraettli, 2022). It is worth noting that most returned mare basalts do not exhibit such strong REE fractionation as seen in the CE-5 samples. If, indeed, the early LMO was crystallizing in equilibrium with garnet, a garnet signature should be more widespread in returned mare basalt samples. Furthermore, abundant garnet crystallization directly from the LMO would lead to lower Sm/Nd in the remaining LMO and later cumulates (Beard et al., 1998), which also contradicts the highly radiogenic Nd isotope compositions of the CE-5 basalt source (Tian et al., 2021). Geochemical modeling also suggests that only limited garnet crystallization (~1.5 %) is required to reproduce the REE patterns of high-K KREEP materials (Neal and Davenport, 2014). Therefore, we propose that garnet crystallization likely had a limited influence on the LMO composition, and the fractionated REE signature in the CE-5 samples was probably not inherited from the LMO stage.

4.4. Residual garnet in the source of CE-5 mare basalts

The discussion above leads us to suggest that the fractionated REE patterns observed in the CE-5 basalts probably reflect unique melting conditions. That is, residual garnet may have played a pivotal role in generating the REE signature in the CE-5 basalts. A similar view was also proposed by Neal (2001) to explain the compositions of some Apollo volcanic glasses. The composition of lunar mantle sources is critical in determining the melting conditions and the characteristics of the melts. Below, we first derive the compositions of a variety of possible sources for mare basalts. Then, we couple phase equilibria modeling and trace element partitioning calculations to constrain the content of residual garnet and the depth of the CE-5 source.

4.4.1. Three source scenarios for CE5 basalts

The major source components of mare basalts are the mantle cumulates formed during LMO solidification and/or subsequent mantle overturn processes (Borg and Carlson, 2023; Hallis et al., 2014; Neal, 2001; Snyder et al., 1992). These cumulates primarily consist of olivine (Ol), orthopyroxene (Opx), clinopyroxene (Cpx), pigeonite (Pgt), ilmenite (Ilm), and garnet (Grt) in varying proportions, with garnet crystallization largely depending on the composition and depth of the LMO. We considered two experimentally derived LMO cumulate sequences: the Taylor Whole Moon (TWM) composition (Schmidt and Kraettli, 2022) and the Lunar Primitive Upper Mantle (LPUM) composition (Rapp and Draper, 2018). Experiments have shown that the common crystallization sequence of major mineral phases follows Ol → Opx → Cpx + Plag ± Pgt→ Qz + Ilm, although the liquid lines of descent vary among different experiments (Rapp and Draper, 2018; Schmidt and Kraettli, 2022). The crystallized cumulate layers can be broadly categorized into three stages:

(1) early Opx-rich cumulates
(2) middle Cpx-rich cumulates
(3) late ilmenite-bearing cumulates (IBC)

Mantle overturn likely led to the mixing of IBC materials to deep cumulates (Borg and Carlson, 2023; Spera, 1992), which may account for the elevated TiO_2 contents of many mare basalts, including the CE-5 basalts (Su et al., 2022). Besides, trapped instantaneous residual liquids (TIRL) may have also been present in the sources (Hallis et al., 2014; Snyder et al., 1992). We thus mixed 5–20 % late-stage IBC and 0–2 % of TIRL with average early Opx-rich cumulates and average middle Cpx-rich cumulates to generate two source scenarios for both LPUM and TWM sequences. Additionally, we followed previous studies (Tian et al., 2021) and considered a third source scenario consisting of an instant middle Cpx-rich cumulate layer at 88 % LMO crystallization for the LPUM sequence and 74.5 % for the TWM sequence, mixed with various

proportions of IBC and TIRL.

To obtain the REE compositions of the mantle sources in each scenario, we performed fractional crystallization calculations based on the mineral phase proportions derived from the experimental studies (Rapp and Draper, 2018; Schmidt and Kraettli, 2022). The initial LMO REE composition was assumed to be that of mean CI chondrites (Palme and Jones, 2003). Once the mantle composition was determined for each scenario (Fig. 4), we calculated the REE compositions of the primary melt by coupling the phase equilibria results and trace element partitioning calculations (See Text S1). Although the absolute REE concentrations of the LMO may differ from those of CI chondrites, they are unfractionated relative to those in the CI chondrites (Snyder et al., 1992; Taylor, 1982). Since our calculations focus on element ratios, this concentration difference has no influence on our discussion below.

In summary, for each LMO model (LPUM or TWM), we obtained the compositions for three scenarios of sources, each comprising cumulates formed at a certain stage of LMO crystallization, mixed with various proportions of IBC and TIRL. These three source scenarios, consisting of 54 compositions in total, cover a wide variety of source compositions for the CE-5 basalts. These potential sources are all depleted with both $(Sm/Yb)_N$ and $(La/Sm)_N$ ratios < 1.1 (Fig. 4), consistent with the Nd isotope results of the CE-5 samples (Tian et al., 2021). One could also consider more complex scenarios by adding a small amount of KREEP in the sources, but again, the Nd isotopes require the sources to be depleted with low $(Sm/Yb)_N$ and $(La/Sm)_N$ ratios. Therefore, the high $(Sm/Yb)_N$ and $(La/Sm)_N$ ratios of the CE-5 basalts probably resulted from the melting processes.

4.4.2. *Garnet content and minimum depth of the CE-5 source*

For each source composition derived above, we performed phase equilibria modeling (Figs. S4-S9) and trace element partitioning calculations to determine the melting conditions needed to generate melts with $(Sm/Yb)_N$ and $(La/Sm)_N$ ratios similar to those observed in the CE-5 basalts, which average 2.1 and 1.4, respectively (See Text S1). In our calculation, we considered a range of melting degrees (0.01–0.03), TIRL contents (0–2 %), and IBC contents (5–20 %). The calculation results for the three source scenarios are presented in Figs. 5, 6, and 7, respectively, assuming TIRL = 1 %, IBC = 5, 10, and 20 %, and a melting degree of 0.02. Results for other TIRL contents (0 and 2 %) and melting degrees (0.01 and 0.03) are provided in Figs. S10-S33. The range of melting degrees considered here (0.01–0.03) is consistent with those constrained by Tian et al. (2021). Extremely low degrees ($F<<0.01$) of partial melting can, in theory, produce elevated $(Sm/Yb)_N$ and $(La/Sm)_N$ ratios as long as the melt is in equilibrium with pyroxene or even olivine. However, extremely low degrees of melting cannot generate sufficient porosity ($>\sim0.01$) required for effective melt extraction (Faul, 1997; Kelemen et al., 1997; Team, 1998; Zhu et al., 2011). In addition, lunar mare basalt sources are thought to contain varying amounts (~1–3 %) of TIRL (Hallis et al., 2014; Snyder et al., 1992), which also suggests that melts at such low fractions cannot escape the source regions. We thus do not consider these extreme low-degree melting conditions.

In the early cumulate source scenario (average Opx-rich cumulates), melts with high $(Sm/Yb)_N$ ratios, similar to those of the CE-5 basalts, can be produced without the need for residual garnet (Fig. 5). This is primarily due to the presence of residual low-Ca pyroxenes (pigeonite and orthopyroxene), which preferentially retain heavy REEs and can fractionate REEs at low melting degrees (Sun and Liang, 2013). However, all melts generated from early cumulate sources are highly depleted in light REEs, resulting in low $(La/Sm)_N$ ratios that do not match the composition of the CE-5 basalts (Fig. 5). These low $(La/Sm)_N$ ratios reflect the depleted nature of the lunar mantle cumulates and the extreme incompatibility of light and middle REEs in Opx, which cannot fractionate $(La/Sm)_N$ efficiently.

Middle cumulate sources (average Cpx-rich cumulates) produce melts with both elevated $(Sm/Yb)_N$ and $(La/Sm)_N$ ratios, closely resembling those of the CE-5 basalts (Fig. 6). The $(Sm/Yb)_N$ ratio strongly correlates with the residual garnet mode, which is, in turn, closely tied to mantle melting pressure (Fig. 6). The results from the third source scenario (instant Cpx-rich cumulate) align with those from the middle cumulate sources (Fig. 7). The amount of IBC in the sources appears to have a limited influence on the residual garnet content and the $(Sm/Yb)_N$ and $(La/Sm)_N$ ratios of the melts. Our results are also insensitive to the amount of TIRL and melting degree (Figs. S10-S33).

The consistent results across a wide variety of source compositions

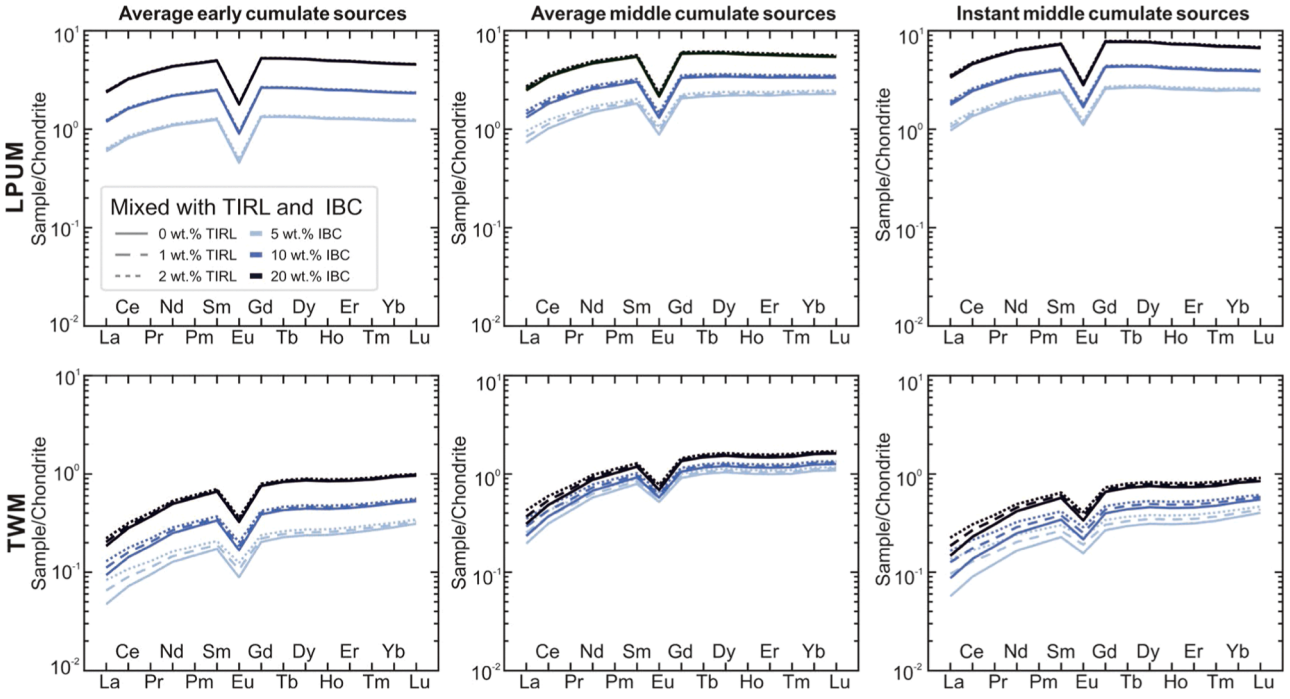


Fig. 4. Source REE patterns (54 in total) of three assumed scenarios for two LMO models (LPUM and TWM). Data are provided in Table S6. Abbreviations: TIRL: trapped instantaneous residual liquids; IBC: Ilmenite-bearing cumulates.

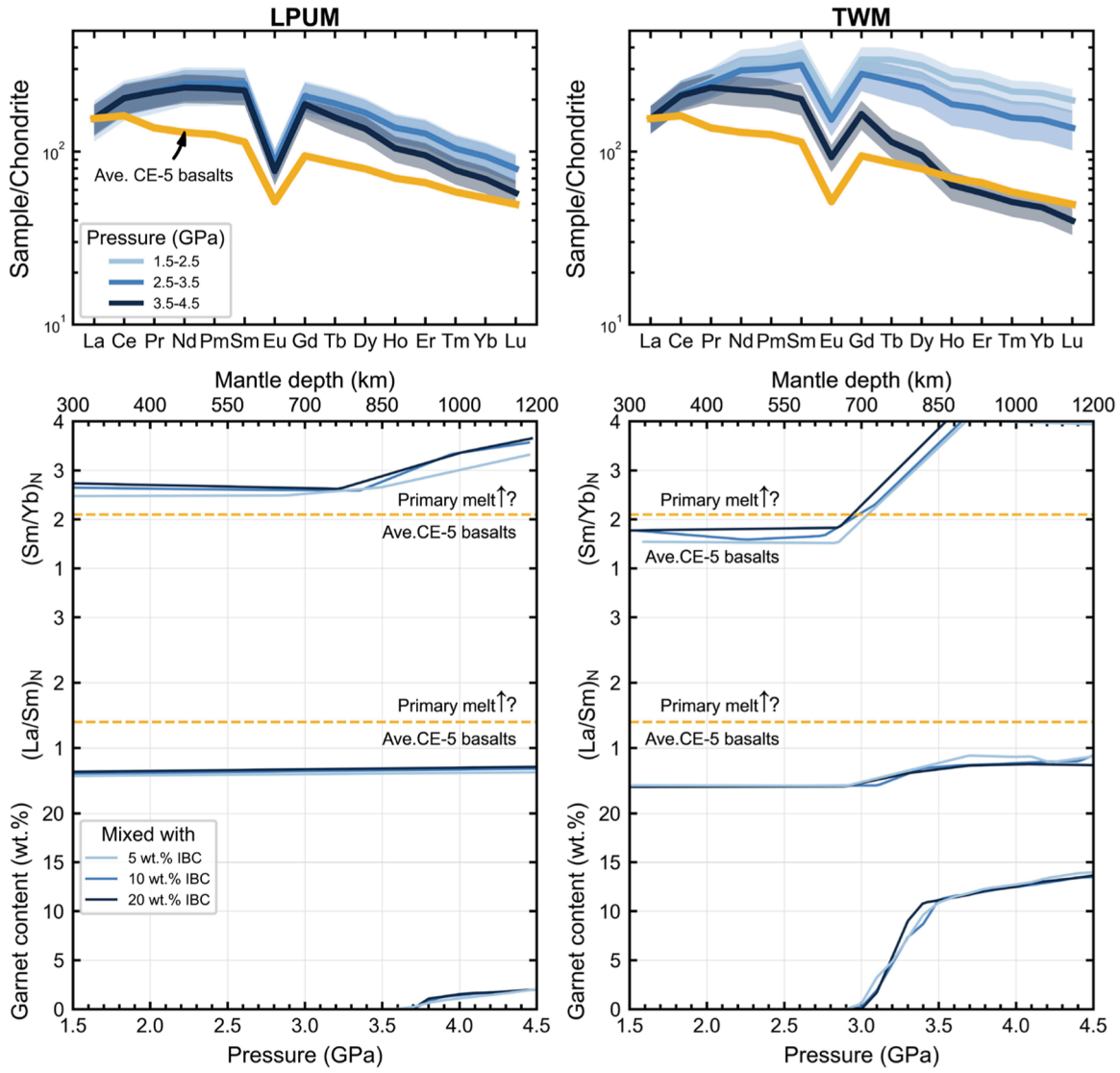


Fig. 5. Results of average early cumulate sources for the two LMO compositions. Shown here are the conditions of TIRL = 1 %, IBC = 5, 10, 20 %, and a melting degree of 0.02. The calculated results of phase equilibria and trace element batch melting are shown in Table S7. The top REE pattern diagrams represent the average REE values across different pressure intervals, with the shaded area indicating two standard errors (2 se). Since the goal of our calculations is to quantify the fractionation between REEs, we normalized our calculated La concentrations to those of the average CE-5 basalts to remove the concentration variations irrelevant to this discussion, and the concentrations of other REE elements are scaled accordingly.

suggest that the pronounced REE fractionation in CE-5 basalts can only be produced in the presence of residual garnet in the deep mantle. The residual garnet content is estimated to be between ~5–10 % (Figs. 6–7). The presence of garnet in the lower lunar mantle is also supported by geophysical studies on the inverted compositional structure of the Moon's interior. For example, lunar laser ranging and seismic data have provided evidence interpreted as indicating a molten zone bearing some garnet in the lowermost mantle (Garcia et al., 2011; Khan et al., 2014; Weber et al., 2011; Zhang et al., 2017). More recently, experimentally determined sound velocity and density models of lunar mantle rocks containing garnet show good agreement with seismic and density profiles at lower mantle depths (Wood et al., 2024). The presence of residual garnet requires high pressures during partial melting. To generate melts with fractionated REE patterns similar to those of the CE-5 basalts, a minimum pressure of approximately 3 GPa is needed (Figs. 6–7), considering that re-equilibration at low pressures could reduce the high $(Sm/Yb)_N$ ratios. This pressure corresponds to a depth of around 700 km or deeper, placing the CE-5 source region in the lunar lower mantle (Figs. 6–7), substantially deeper than the sources of the older mare basalts with lower $(Sm/Yb)_N$ ratios sampled by the Apollo missions and previously reported for the CE-5 basalts (Heiken et al., 1991; Longhi, 1992; Luo et al., 2023).

Our findings offer a different perspective from previous studies, all of which proposed a CE-5 source in the lunar upper mantle. These earlier studies inferred the melting depth by evaluating pressure ranges derived from either multiple saturation point (MSP) in assumed primary magmas (Haupt et al., 2023; Su et al., 2022; Wang et al., 2024a) or thermobarometers based on CE-5 mineral compositions (Luo et al., 2023; Wang et al., 2024a). The MSP approach is highly sensitive to the primary melt composition, which is usually assumed and has large uncertainties. On the other hand, the CE-5 basalts are substantially evolved and their mineral compositions may not capture the conditions of early differentiation or source melting. The susceptibility of both magma and mineral compositions to differentiation has led to ongoing discussions regarding the use of MSP and mineral-based thermobarometers as proxies for magma source pressures (Asimow and Longhi, 2004; Neal, 2001), which can introduce uncertainties into depth estimates. By contrast, our study leverages trace element ratios ($(Sm/Yb)_N$), which are

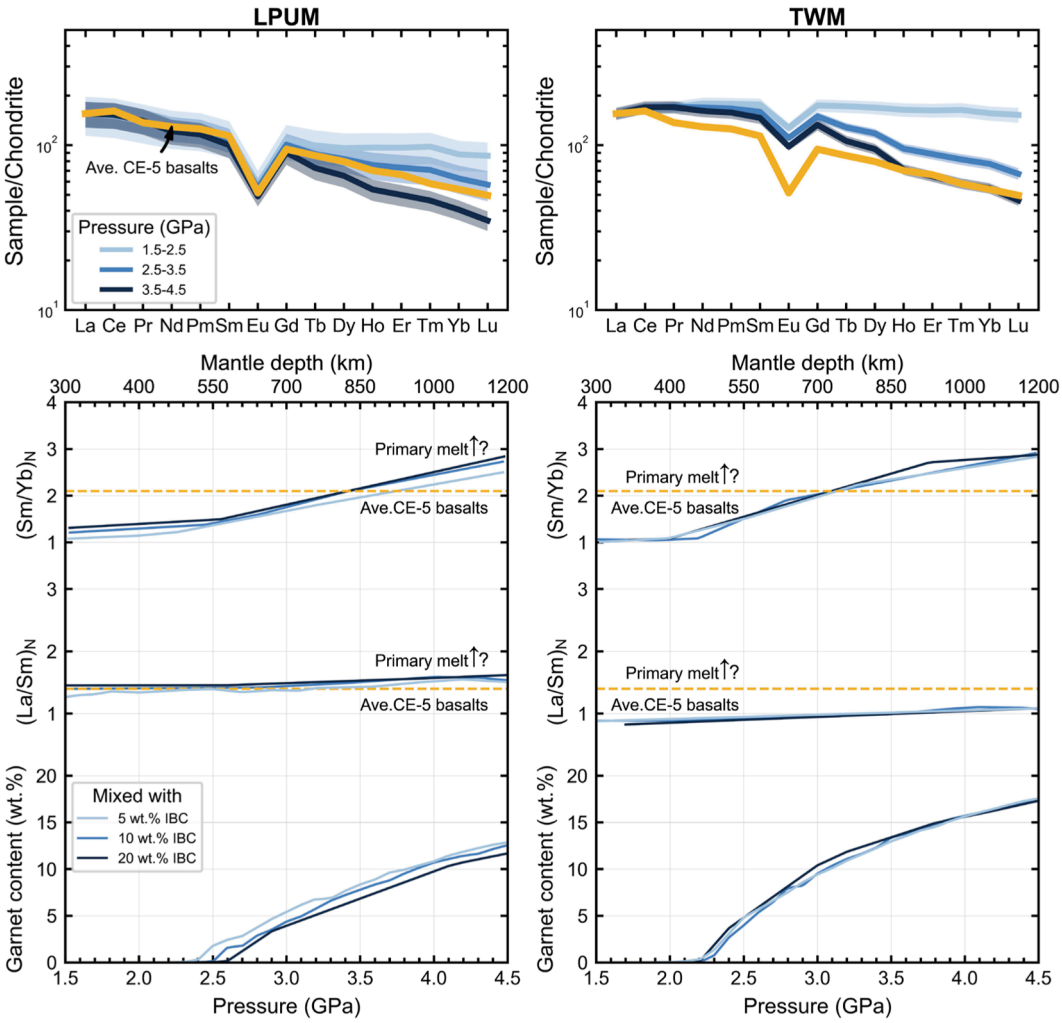


Fig. 6. Results of average middle cumulate sources for the two LMO compositions. Shown here are the conditions of TIRL = 1 %, IBC = 5, 10, 20 %, and a melting degree of 0.02. The calculated results of phase equilibria and trace element batch melting are shown in Table S7. The data processing method in the top REE pattern diagrams is the same as in Fig. 5.

less influenced by crystal fractionation at shallow depths, along with phase equilibrium modeling of lunar mantle melting, to provide more robust constraints on the CE-5 origin depth.

4.5. *Melt ascending from the lunar lower mantle?*

One difficulty with the ultra-deep source scenario proposed here is whether the melt can be segregated from the residues and rise through the thick mantle above. There are many aspects to explore to fully address this question, which is beyond the scope of this paper and worth additional efforts in the future. Here, we examine the density contrast between the melt and the residue, which is critical for the melt to ascend from the source region (Guenther et al., 2022). We derived the densities of the melts and residues from our phase equilibria modeling. For both average and instantaneous Cpx-rich cumulate source scenarios, our results indicate that the melts are less dense than their residual sources up to 4 GPa or higher pressures (Figs. S34-S42). In addition to melt-residue density contrast at the source, successful ascent requires the melt to be buoyant relative to the surrounding mantle column. To assess this buoyancy issue, we calculated liquid density–depth profiles for melts generated at ~3.0 and 4.0 GPa and compared them with proposed lunar mantle density profiles (Garcia et al., 2019; Weber et al., 2011; Wood et al., 2024) (Fig. 8). The CE-5 magmas are inferred to have stalled at shallow crustal depths (~2–5 kbar), where they evolved through high-degree fractional crystallization (Luo et al., 2023). We therefore assumed limited fractional crystallization of the primary melts during their ascent from the deep-seated sources. We tracked the density evolution of the primary melts along their liquidus during ascent via phase equilibria modeling. As variations in TIRL content (0, 1, 2 %) and degree of melting (0.01–0.03) have minimal effects on melt composition, density–depth calculations were performed using representative models with TIRL = 1 % and a melting degree of 0.02 (Table S8). Our results suggest that melts initially formed at 3.0 and even 4.0 GPa are buoyant relative to the mantle column during the entire ascending path (Fig. 8).

Buoyancy is only one aspect to understand how magmas may ascend from the deep lunar mantle. Future efforts may explore the density contrast between an evolving melt and more complex mantle columns, magma ascent mechanisms (porous flow, diking, and/or diapir), and mantle thermal conditions needed to prevent freezing of the magmas.

5. Implications

The Moon is expected to have cooled rapidly after its formation (Shearer et al., 2006), yet the prolonged volcanism remains a puzzling phenomenon. Our findings of a lunar lower mantle origin for the CE-5 basalts lead to two hypotheses. Firstly, mantle convection may have persisted in the deep lunar mantle until at least two billion years ago, triggering decompression melting in upwelling zones (Fig. 9). The IBC

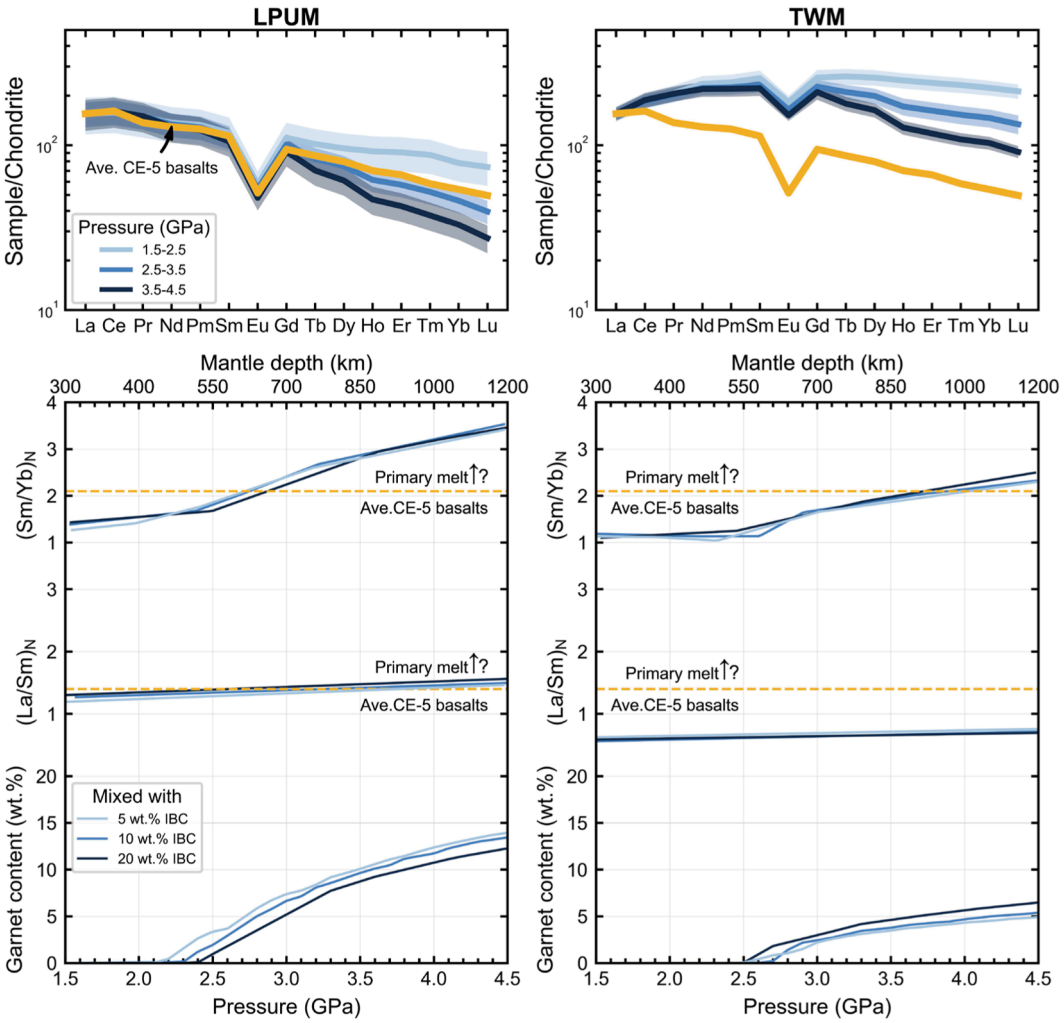


Fig. 7. Results of instant Cpx-rich cumulate sources for the two LMO compositions. Shown here are the conditions of TIRL = 1 %, IBC = 5, 10, 20 %, and a melting degree of 0.02. The calculated results of phase equilibria and trace element batch melting are shown in Table S7. The data processing method in the top REE pattern diagrams is the same as in Fig. 5.

layer formed during the late stage of LMO crystallization and was enriched in heat-producing elements (K, Th, and U) due to the presence of trapped late-stage melt (Hess and Parmentier, 1995; Li et al., 2019). The IBC layer was gravitationally unstable and thus sunk to the lunar core-mantle boundary (Borg and Carlson, 2023; Hess and Parmentier, 1995; Li et al., 2019; Liang et al., 2024; Zhao et al., 2019). While earlier studies favored weak or absent lunar convection (Pritchard and Stevenson, 2000; Shearer et al., 2006), the heat-producing elements carried down by the IBC materials may have resulted in sustained heating of the lowermost mantle, driving convection in at least the deep lunar mantle (Borg and Carlson, 2023; Laneuville et al., 2018; Liang et al., 2024). Recent paleomagnetic studies of CE-5 basalts suggest a weak dynamo during their formation (Cai et al., 2025), indicating the presence of thermal convection in the deep lunar interior during the later stages of the Moon's evolution. However, this interpretation remains debated, as earlier studies argued that the Moon did not possess a long-lived core dynamo, and that the remanent magnetization of lunar regolith instead reflects ion transport from the solar wind and Earth's magnetosphere (Tarduno et al., 2021). Thermally driven convective upwelling in the deep mantle might entrain a small amount of IBC materials, serving as a possible source for the CE-5 basalts (Shearer et al., 2006; Su et al., 2022). Another important consequence of the IBC-induced overturn is the mantle-scale mass redistribution. This process could have transported the shallowly formed Cpx-rich cumulates into the lower mantle (Borg and Carlson, 2023; Li et al., 2019; Liang et al., 2024), which later became the major source components of the CE-5 basalts indicated by our findings.

Another possibility is that the CE-5 magma may have tapped a melt-bearing layer near the core-mantle boundary (Fig. 9). Geophysical inverse analyses combined with phase equilibrium modeling suggest the existence of a partially molten zone, likely containing some garnet, in the lowermost mantle just above the lunar core (Khan et al., 2014; Weber et al., 2011). The U, Th, and K-rich IBC materials, accumulated at the core-mantle boundary, may have triggered direct melting at the lunar core-mantle boundary by radiogenic heating, and this melt layer may have persisted to the present (Khan et al., 2014). This scenario is also consistent with thermal evolution modeling (Zhang et al., 2013). Depending on their FeO and TiO_2 contents, and thus densities, melts with lower densities could rise and serve as the primary sources of CE-5 basalts (Khan et al., 2014; Li et al., 2019). More recent studies of the Moon's yearly gravity change due to tides further suggest that only models with a soft layer, potentially a melt-bearing layer, at the bottom of the mantle match current observations (Goossens et al., 2024).

CRediT authorship contribution statement

Runwu Li: Writing – original draft, Investigation, Data curation, Conceptualization. **Ming Tang:** Writing – review & editing, Project

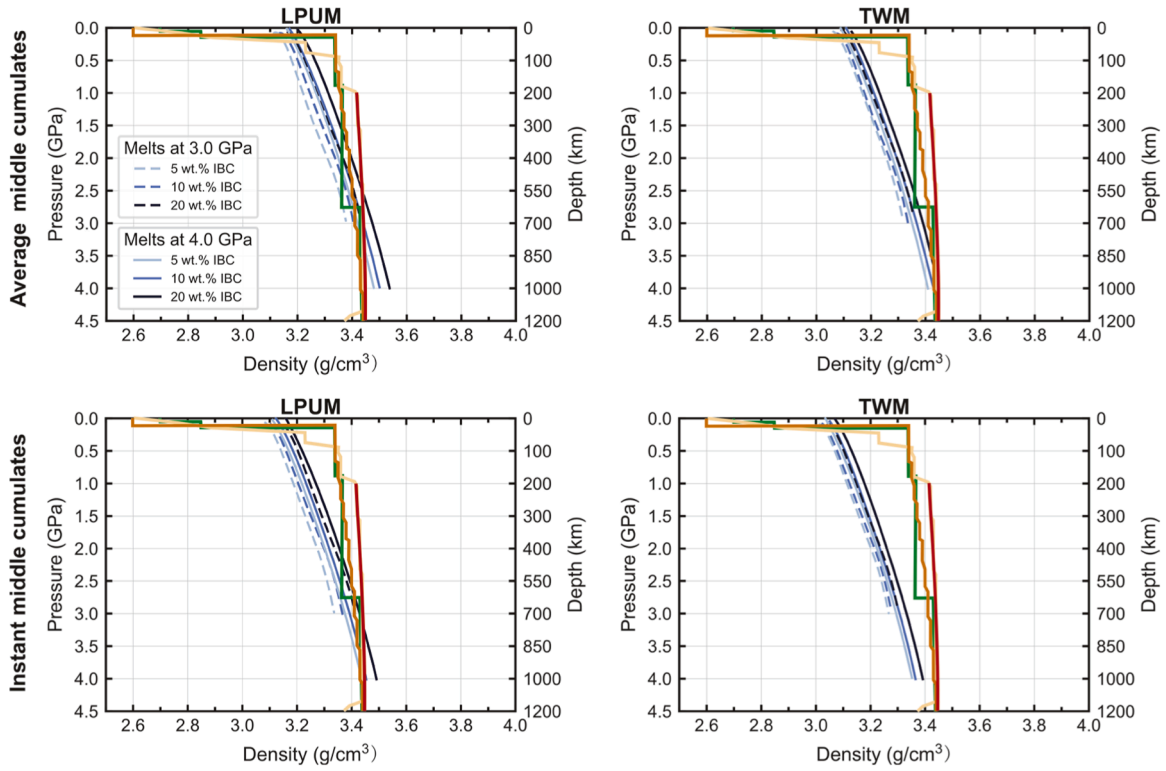


Fig. 8. Calculated liquid density profiles for melts formed at 3.0 and 4.0 GPa for both average and instant middleCpx-rich cumulate source scenarios. Shown here are the source conditions of TIRL = 1 %, IBC = 5, 10, 20 %, and a melting degree of 0.02. The green, orange, and red curves represent the lunar mantle density profiles from Weber et al. (2011); Garcia et al. (2019), and Wood et al. (2024), respectively.

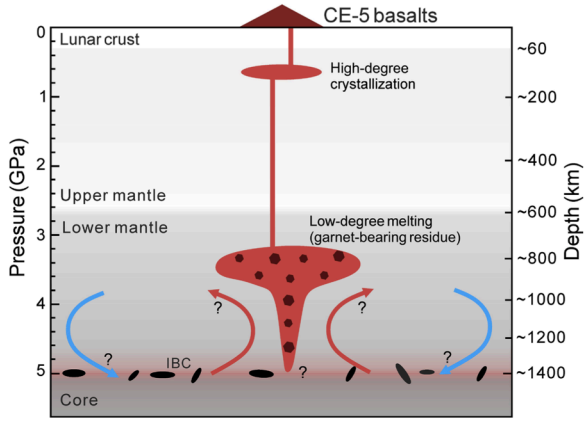


Fig. 9. A schematic diagram (not to scale) illustrating the formation of the young CE-5 basalts, from melting in lunar lower mantle to shallow crystallization and eruption. Abbreviations: IBC: Ilmenite-bearing cumulates.

administration, Investigation, Funding acquisition, Conceptualization. **Jiaxi Wang:** Methodology, Investigation, Data curation.

Declaration of competing interest

The authors declare that they have no known competing financial interests or personal relationships that could have appeared to influence the work reported in this paper.

Acknowledges

We gratefully acknowledge the China National Space Administration (CNSA) for providing the CE-5 samples. This research was supported by the National Natural Science Foundation of China (Grant No. 42125302). We thank the two anonymous reviewers for their constructive comments, which significantly improved the manuscript, and Editor Fangzhen Teng for his thoughtful editorial handling. M.T. acknowledges support from the New Cornerstone Science Foundation through the XPLORER PRIZE. We also thank Hao Chen and Jintuan Wang for their insightful discussions.

Supplementary materials

Supplementary material associated with this article can be found, in the online version, at doi:10.1016/j.epsl.2025.119650.

Data availability

Data will be made available on request.

References

Asimow, P.D., Longhi, J., 2004. The significance of multiple saturation points in the context of polybaric near-fractional melting. J. Petrol. 45, 2349–2367.
Beard, B.L., Taylor, L.A., Scherer, E.E., Johnson, C.M., Snyder, G.A., 1998. The source region and melting mineralogy of high-titanium and low-titanium lunar basalts deduced from Lu-Hf isotope data. Geochim. Cosmochim. Acta 62, 525–544.
Borg, L.E., Carlson, R.W., 2023. The evolving chronology of moon formation. Annu. Rev. Earth Planet. Sci. 51, 25–52.
Cai, S., Qin, H., Wang, H., Deng, C., Yang, S., Xu, Y., Zhang, C., Tang, X., Gu, L., Li, X., Shen, Z., Zhang, M., He, K., Qi, K., Fan, Y., Dong, L., Hou, Y., Shi, P., Liu, S., Su, F., Chen, Y., Li, Q., Li, J., Mitchell, R.N., He, H., Li, C., Pan, Y., Zhu, R., 2025. Persistent but weak magnetic field at the moon's midstage revealed by Chang'e-5 basalt. Sci. Adv. 11, eadp3333.
Che, X., Nemchin, A., Liu, D., Long, T., Wang, C., Norman, M.D., Joy, K.H., Tartese, R., Head, J., Jolliff, B., Snape, J.F., Neal, C.R., Whitehouse, M.J., Crow, C., Benedix, G., Jourdan, F., Yang, Z., Yang, C., Liu, J., Xie, S., Bao, Z., Fan, R., Li, D., Li, Z., Webb, S. G., 2021. Age and composition of young basalts on the moon, measured from samples returned by Chang'e-5. Science 374, 887–890.

Chen, K., Tang, M., Hu, Z., Liu, Y., 2023. Generation of tholeiitic and calc-alkaline arc magmas and its implications for continental growth. Geochim. Cosmochim. Acta 355, 173–183.
Elardo, S.M., Draper, D.S., Shearer, C.K., 2011. Lunar magma ocean crystallization revisited: bulk composition, early cumulate mineralogy, and the source regions of the highlands Mg-suite. Geochim. Cosmochim. Acta 75, 3024–3045.
Faul, U.H., 1997. Permeability of partially molten upper mantle rocks from experiments and percolation theory. J. Geophys. Res. 102, 10299–10311.
Garcia, R.F., Gagnepain-Beyneix, J., Chevrot, S., Lognonné, P., 2011. Very preliminary reference moon model. Phys. Earth Planet. Inter. 188, 96–113.
Garcia, R.F., Khan, A., Drilleau, M., Margerin, L., Kawamura, T., Sun, D., Wieczorek, M. A., Rivoldini, A., Nunn, C., Weber, R.C., Marusiak, A.G., Lognonné, P., Nakamura, Y., Zhu, P., 2019. Lunar seismology: an update on interior structure models. Space Sci. Rev. 215, 50.
Goossens, S., Matsuyama, I., Cascioli, G., Mazarico, E., 2024. A low-viscosity lower lunar mantle implied by measured monthly and yearly tides. AGU Adv. 5, e2024AV001285.
Grove, T., Walker, D., Longhi, J., Stolper, E., Hays, J., 1973. Petrology of rock 12002 and origin of picritic basalts at Oceanus Procellarum. In: Proc. 4th Lunar Sci. Conf, 4.
Gualda, G.A.R., Ghiorso, M.S., Lemons, R.V., Carley, T.L., 2012. Rhyolite-MELTS: a modified calibration of MELTS optimized for silica-rich, fluid-bearing magmatic systems. J. Petrol. 53, 875–890.
Guenther, M.E., Brown Krein, S.M., Grove, T.L., 2022. The influence of variable oxygen fugacity on the source depths of lunar high-titanium ultramafic glasses. Geochim. Cosmochim. Acta 334, 217–230.
Hallis, L.J., Anand, M., Strekopytov, S., 2014. Trace-element modelling of mare basalt parental melts: implications for a heterogeneous lunar mantle. Geochim. Cosmochim. Acta 134, 289–316.
Haupt, C.P., Renggli, C.J., Klaver, M., Steenstra, E.S., Berndt, J., Rohrbach, A., Klemme, S., 2023. Experimental and petrological investigations into the origin of the lunar Chang'e 5 basalts. Icarus 402, 115625.
Heiken, G., Vaniman, D., French, B.M., 1991. Lunar Sourcebook: a User's Guide to the Moon. Cambridge University Press, Cambridge [England].
Hess, P.C., Parmentier, E.M., 1995. A model for the thermal and chemical evolution of the moon's interior: implications for the onset of mare volcanism. Earth Planet. Sci. Lett. 134, 501–514.
Hu, S., He, H., Ji, J., Lin, Y., Hui, H., Anand, M., Tartèse, R., Yan, Y., Hao, J., Li, R., Gu, L., Guo, Q., He, H., Ouyang, Z., 2021. A dry lunar mantle reservoir for young mare basalts of Chang'e-5. Nature 600, 49–53.
Jing, J.-J., Lin, Y., Knibbe, J.S., van Westrenen, W., 2022. Garnet stability in the deep lunar mantle: constraints on the physics and chemistry of the interior of the moon. Earth Planet. Sci. Lett. 584, 117491.
Jochum, K.P., Stoll, B., Herwig, K., Willbold, M., Hofmann, A.W., Amini, M., Aarburg, S., Abouchami, W., Hellebrand, E., Mocek, B., Raczek, I., Stracke, A., Alard, O., Bouman, C., Becker, S., Dücking, M., Brätz, H., Klemd, R., de Bruin, D., Canil, D., Cornell, D., de Hoog, C.J., Dalpé, C., Danyushevsky, L., Eisenhauer, A., Gao, Y., Snow, J.E., Groschopf, N., Günther, D., Latkoczy, C., Guillong, M., Hauri, E.H., Höfer, H.E., Lahaye, Y., Horz, K., Jacob, D.E., Kasemann, S.A., Kent, A.J.R., Ludwig, T., Zack, T., Mason, P.R.D., Meixner, A., Rosner, M., Misawa, K., Nash, B.P., Pfänder, J., Premo, W.R., Sun, W.D., Tiepolo, M., Vannucci, R., Vennemann, T., Wayne, D., Woodhead, J.D., 2006. MPI-DING reference glasses for in situ microanalysis: new reference values for element concentrations and isotope ratios. Geochem. Geophys. Geosystems 7.
Johnson, T.E., Morrissey, L.J., Nemchin, A.A., Gardiner, N.J., Snape, J.F., 2021. The phases of the moon: modelling crystallisation of the lunar magma ocean through equilibrium thermodynamics. Earth Planet. Sci. Lett. 556, 116721.
Kelemen, P.B., Hirth, G., Shimizu, N., Spiegelman, M., Dick, H.J.B., 1997. A review of melt migration processes in the adiabatically upwelling mantle beneath oceanic spreading ridges. Philos. Trans. R. Soc. Lond. A 355, 283–318.
Khan, A., Connolly, J.A.D., Pommier, A., Noir, J., 2014. Geophysical evidence for melt in the deep lunar interior and implications for lunar evolution. J. Geophys. Res. 119, 2197–2221.
Laneuville, M., Taylor, J., Wieczorek, M.A., 2018. Distribution of radioactive heat sources and thermal history of the moon. J. Geophys. Res. 123, 3144–3166.
Lee, C.-T., Sun, C., Sharton-Bierig, E., Phelps, P., Borchardt, J., Liu, B., Costin, G., Johnston, A., 2022. Widespread phosphorous excess in olivine, rapid crystal growth, and implications for magma dynamics. Volcanica 5, 433–450.
Li, C., Hu, H., Yang, M.-F., Pei, Z.-Y., Zhou, Q., Ren, X., Liu, B., Liu, D., Zeng, X., Zhang, G., Zhang, H., Liu, J., Wang, Q., Deng, X., Xiao, C., Yao, Y., Xue, D., Zuo, W., Su, Y., Wen, W., Ouyang, Z., 2021a. Characteristics of the lunar samples returned by the Chang'E-5 mission. Natl. Sci. Rev. 9.
Li, H., Zhang, N., Liang, Y., Wu, B., Dygert, N.J., Huang, J., Parmentier, E.M., 2019. Lunar cumulate mantle overturn: a model constrained by ilmenite rheology. J. Geophys. Res. 124, 1357–1378.
Li, Q.-L., Zhou, Q., Liu, Y., Xiao, Z., Lin, Y., Li, J.-H., Ma, H.-X., Tang, G.-Q., Guo, S., Tang, X., Yuan, J.-Y., Li, J., Wu, F.-Y., Ouyang, Z., Li, C., Li, X.-H., 2021b. Two-billion-year-old volcanism on the moon from Chang'e-5 basalts. Nature 600, 54–58.
Liang, W., Broquet, A., Andrews-Hanna, J.C., Zhang, N., Ding, M., Evans, A.J., 2024. Vestiges of a lunar ilmenite layer following mantle overturn revealed by gravity data. Nat. Geosci. 17, 361–366.
Liu, Y.S., Hu, Z.C., Gao, S., Günther, D., Xu, J., Gao, C.G., Chen, H.H., 2008. In situ analysis of major and trace elements of anhydrous minerals by LA-ICP-MS without applying an internal standard. Chem. Geol. 257, 34–43.
Longhi, J., 1992. Experimental petrology and petrogenesis of mare volcanics. Geochim. Cosmochim. Acta 56, 2235–2251.
Luo, B., Wang, Z., Song, J., Qian, Y., He, Q., Li, Y., Head, J.W., Moynier, F., Xiao, L., Becker, H., Huang, B., Ruan, B., Hu, Y., Pan, F., Xu, C., Liu, W., Zong, K., Zhao, J., Zhang, W., Hu, Z., She, Z., Wu, X., Zhang, H., 2023. The magmatic architecture and evolution of the Chang'e-5 lunar basalts. Nat. Geosci. 16, 301–308.
Neal, C., 2001. Interior of the moon: the presence of garnet in the primitive deep lunar mantle. J. Geophys. Res. 106, 27865–27885.
Neal, C.R., Davenport, J.D., 2014. Trace element evolution of the lunar magma ocean, the origin of KREEP, and the influence of garnet. In: 45th Annual Lunar and Planetary Science Conference. Texas. The Woodlands, p. 1181.
Neal, C.R., Taylor, L.A., 1992. Petrogenesis of mare basalts: a record of lunar volcanism. Geochim. Cosmochim. Acta 56, 2177–2211.
Palme, H., Jones, A., 2003. 1.03 - solar system abundances of the elements. In: Holland, H.D., Turekian, K.K. (Eds.), Treatise On Geochemistry. Pergamon, Oxford, pp. 41–61.
Pritchard, M., Stevenson, D., 2000. Thermal aspects of a lunar origin by giant impact. Orig. Earth Moon.
Rapp, J.F., Draper, D.S., 2018. Fractional crystallization of the lunar magma ocean: updating the dominant paradigm. Meteorit. Planet. Sci. 53, 1432–1455.
Schmidt, M.W., Kraettli, G., 2022. Experimental crystallization of the lunar magma ocean, initial selenotherm and density stratification, and implications for crust formation, overturn and the bulk silicate moon composition. J. Geophys. Res. 127, e2022JE007187.
Shearer, C.K., Hess, P.C., Wieczorek, M.A., Pritchard, M.E., Parmentier, E.M., Borg, L.E., Longhi, J., Elkins-Tanton, L.T., Neal, C.R., Antonenko, I., Canup, R.M., Halliday, A. N., Grove, T.L., Hager, B.H., Lee, D.-C., Wiechert, U., 2006. Thermal and magmatic evolution of the moon. Rev. Mineral. Geochem. 60, 365–518.
Snape, J.F., Nemchin, A.A., Whitehouse, M.J., Merle, R.E., Hopkinson, T., Anand, M., 2019. The timing of basaltic volcanism at the Apollo landing sites. Geochim. Cosmochim. Acta 266, 29–53.
Snyder, G.A., Taylor, L.A., Neal, C.R., 1992. A chemical model for generating the sources of mare basalts: combined equilibrium and fractional crystallization of the lunar magmasphere. Geochim. Cosmochim. Acta 56, 3809–3823.
Spera, F.J., 1992. Lunar magma transport phenomena. Geochim. Cosmochim. Acta 56, 2253–2265.
Spohn, T., Konrad, W., Breuer, D., Ziethe, R., 2001. The longevity of lunar volcanism: implications of thermal evolution calculations with 2D and 3D mantle convection models. Icarus 149, 54–65.
Su, B., Yuan, J., Chen, Y., Yang, W., Mitchell, R.N., Hui, H., Wang, H., Tian, H., Li, X.-H., Wu, F.-Y., 2022. Fusible mantle cumulates trigger young mare volcanism on the cooling moon. Sci. Adv. 8, eabn2103.
Su, B., Zhang, D., Chen, Y., Yang, W., Mao, Q., Li, X.-H., Wu, F.-Y., 2023. Low Ni and Co olivine in Chang'E-5 basalts reveals the origin of the young volcanism on the moon. Sci. Bull. 68, 1918–1927.
Sun, C., Liang, Y., 2013. Distribution of REE and HFSE between low-Ca pyroxene and lunar picritic melts around multiple saturation points. Geochim. Cosmochim. Acta 119, 340–358.
Sun, S.S., McDonough, W.F., 1989. Chemical and isotopic systematics of oceanic basalts: implications for mantle composition and processes. Geol. Soc. Spec. Publ. 42, 313–345.
Tang, M., Ji, W.-Q., Chu, X., Wu, A., Chen, C., 2020. Reconstructing crustal thickness evolution from europium anomalies in detrital zircons. Geology 49, 76–80.
Tarduno, J.A., Cottrell, R.D., Lawrence, K., Bono, R.K., Huang, W., Johnson, C.L., Blackman, E.G., Smirnov, A.V., Nakajima, M., Neal, C.R., Zhou, T., Ibanez-Mejia, M., Oda, H., Crummins, B., 2021. Absence of a long-lived lunar paleomagnetosphere. Sci. Adv. 7, eabi7647.
Taylor, S.R., 1982. Planetary Science: A LUNAR PERSPECTIVE. Lunar and Planetary Institute Houston.
Team, T.M.S., 1998. Imaging the deep seismic structure beneath a mid-ocean ridge: the MELT experiment. Science 280, 1215–1218.
Tian, H.-C., Wang, H., Chen, Y., Yang, W., Zhou, Q., Zhang, C., Lin, H.-L., Huang, C., Wu, S.-T., Jia, L.-H., Xu, L., Zhang, D., Li, X.-G., Chang, R., Yang, Y.-H., Xie, L.-W., Zhang, D.-P., Zhang, G.-L., Yang, S.-H., Wu, F.-Y., 2021. Non-KREEP origin for Chang'e-5 basalts in the procellarum KREEP Terrane. Nature 600, 59–63.
Wang, C., Xu, Y.-G., Zhang, L., Chen, Z., Xia, X., Lin, M., Guo, F., 2024a. A shallow (<100 km) ilmenite-bearing pyroxenitic source for young lunar volcanism. Earth Planet. Sci. Lett. 639, 118770.
Wang, Z., Zong, K., Li, Y., Li, J., He, Q., Zou, Z., Becker, H., Moynier, F., Day, J.M.D., Zhang, W., Qian, Y., Xiao, L., Hu, Z., She, Z., Hui, H., Wu, X., Liu, Y., 2024b. Young KREEP-like mare volcanism from oceanus procellarum. Geochim. Cosmochim. Acta 373, 17–34.
Warren, P.H., 1989. KREEP: major-element diversity, trace-element uniformity (almost). In: Taylor, G.J., Warren, P.H. (Eds.), Moon in Transition: Apollo 14, KREEP, and Evolved Lunar Rocks, pp. 149–153.
Warren, P.H., Taylor, G.J., 2014. The moon. In: T, H.D., H., K.K. (Ed.), Treatise On Geochemistry, 2nd Edition. Elsevier, Oxford, pp. 213–250.
Warren, P.H., Wasson, J.T., 1979. The origin of KREEP. Rev. Geophys. 17, 73–88.
Watson, E.B., Müller, T., 2009. Non-equilibrium isotopic and elemental fractionation during diffusion-controlled crystal growth under static and dynamic conditions. Chem. Geol. 267, 111–124.
Weber, R.C., Lin, P.-Y., Garnero, E.J., Williams, Q., Lognonné, P., 2011. Seismic detection of the lunar core. Science 331, 309–312.
Wieczorek, M., Jolliff, B., Khan, A., Pritchard, M., Weiss, B., Williams, J., Hood, L., Righter, K., Neal, C., Shearer, C., McCallum, I., Tompkins, S., Hawke, B., Peterson, C., Gillis, J., Bussey, B., 2006. The constitution and structure of the lunar interior. Rev. Mineral. Geochem. 60, 221–364.

Wood, M.C., Gréaux, S., Kono, Y., Kakizawa, S., Ishikawa, Y., Inoué, S., Kuwahara, H., Higo, Y., Tsujino, N., Irifune, T., 2024. Sound velocities in lunar mantle aggregates at simultaneous high pressures and temperatures: implications for the presence of garnet in the deep lunar interior. Earth Planet. Sci. Lett. 641, 118792.

Wu, S., Audétat, A., Jochum, K.P., Wang, H., Chen, J., Stoll, B., Zhang, C., Bao, Z., Yang, S., Li, C., Wang, X., Xu, C., Xu, L., Huang, C., Xie, L., Yang, Y., Yang, J., 2022. Three natural andesitic to rhyolitic glasses (OJY-1, OH-1, OA-1) as reference materials for in situ microanalysis. Geostand. Geoanalytical Res. 46, 673–700.

Wu, S., Wörner, G., Jochum, K.P., Stoll, B., Simon, K., Kronz, A., 2019. The preparation and preliminary characterisation of three synthetic andesite reference glass materials (ARM-1, ARM-2, ARM-3) for in situ microanalysis. Geostand. Geoanalytical Res. 43, 567–584.

Zhang, N., Dygert, N., Liang, Y., Parmentier, E.M., 2017. The effect of ilmenite viscosity on the dynamics and evolution of an overturned lunar cumulate mantle. Geophys. Res. Lett. 44, 6543–6552.

Zhang, N., Parmentier, E.M., Liang, Y., 2013. A 3-D numerical study of the thermal evolution of the moon after cumulate mantle overturn: the importance of rheology and core solidification. J. Geophys. Res. 118, 1789–1804.

Zhao, Y., de Vries, J., van den Berg, A.P., Jacobs, M.H.G., van Westrenen, W., 2019. The participation of ilmenite-bearing cumulates in lunar mantle overturn. Earth Planet. Sci. Lett. 511, 1–11.

Zhu, W., Gaetani, G.A., Fusseis, F., Montési, L.G.J., De Carlo, F., 2011. Microtomography of partially molten rocks: three-dimensional melt distribution in mantle peridotite. Science 332, 88–91.

Zong, K., Wang, Z., Li, J., He, Q., Li, Y., Becker, H., Zhang, W., Hu, Z., He, T., Cao, K., She, Z., Wu, X., Xiao, L., Liu, Y., 2022. Bulk compositions of the Chang'E-5 lunar soil: insights into chemical homogeneity, exotic addition, and origin of landing site basalts. Geochim. Cosmochim. Acta 335, 284–296.